DYNAMIC IMAGE RECONSTRUCTION USING TEMPORALLY ADAPTIVE REGULARIZATION FOR EMISSION TOMOGRAPHY

Mingwu Jin, Yongyi Yang, and Miles N. Wernick

Dept. Electrical and Computer Engineering
Illinois Institute of Technology
Chicago, IL 60616, USA

ABSTRACT

Temporal basis functions have been found to be effective for regularizing the time-varying image activities in dynamic emission tomography. By modelling the tracer distribution function at individual pixels as a linear combination of a set of basis functions, the reconstruction problem becomes that of estimating the weights of the basis functions. In this work, we explore the use of temporally adaptive regularization in the basis function domain, where spatial smoothing is enforced in an adaptive fashion according to the time-varying data statistics. In our experiments the proposed method was demonstrated using simulated Tc99m-Teboroxime SPECT imaging with the gated mathematical cardiac-torso (gMCAT) phantom. Our results show that the proposed approach can lead to more accurate reconstruction of the time activities, which is important for differentiation between a perfusion defect and the normal myocardium.

Index Terms— Dynamic reconstruction, emission tomography, temporal basis functions, adaptive regularization

1. INTRODUCTION

Dynamic imaging with emission tomography usually deals with reconstruction of a series of image frames during the course of data acquisition, which are useful for characterizing the time-varying tracer distribution within the body. Due to the limited data counts, there exists a trade-off between temporal resolution and imaging noise in the reconstructed frames. This is particularly serious in SPECT where the available projection data may not even be complete for reconstruction at any time instance.

In recent years several reconstruction methods have been developed to deal with these challenges, where temporal basis functions are found to be effective for regularizing the time activities at individual pixels. By modelling the tracer distribution function as a linear combination of a set of basis functions, the reconstruction problem simply becomes that of estimating the weights of the basis functions. For example, in [1] exponential functions are used for reconstruction from list mode PET data. In [2]–[4] pre-defined B-spline basis functions are used. In [5], [6] the basis functions are estimated from the data by using the Karhunen-Loève (KL) transform. Alternatively, in [7], [8] the temporal activities of the tracer are restricted to only four types: constant, increasing only, decreasing only, or first increasing then decreasing.

In our previous work [9], [10], we applied B-spline basis functions for reconstruction of dynamic cardiac gated SPECT. In a gated acquisition, the data counts are further divided into a number of gate intervals. Thus, the imaging noise will be even more pronounced. Owing to the elevated noise in this problem, we introduced a regularization prior to impose additional spatial smoothing on the reconstructed weights of the B-splines. This was found to be effective for further noise reduction.

In [9], [10], the weights of the B-splines were treated in a uniform fashion in the smoothing prior. In this paper, we extend this work by refining this prior so that spatial smoothing will be imposed in an adaptive fashion in the basis function domain according to the time-varying data statistics. In our experiments we demonstrated the proposed method using simulated cardiac SPECT. However, our method is general and should be equally applicable to other dynamic imaging modalities such as PET.

We note that in the literature there also exists an alternative reconstruction approach in dynamic imaging, which aims to reconstruct kinetic parameters directly from the projection data [11]–[14]. In this paper we focus on reconstruction of dynamic images. The rest of the paper is organized as follows: in Section 2 we describe the dynamic imaging model; in Section 3 we present our regularized reconstruction method. Evaluation study and results are given in Section 4, and conclusions are given in Section 5.

2. DYNAMIC IMAGING MODEL

In dynamic imaging, the tracer distribution is reconstructed by binning the acquired data acquisition over a series of time intervals. Assume that a total of S time intervals (i.e., frames) are used. The imaging model can be written as:

$$E[g_t] = H_t f_t,\ t = 1, \ldots, S \tag{1}$$

This work was supported by the National Institutes of Health under grant HL65425.

where g_t, H_t, and f_t are the projection data, the system matrix, and the tracer distribution, respectively, during binning interval t, $E[\cdot]$ is the expectation operator. Assuming M bins in the detector, and N pixels for f_t, then g_t is an $M \times 1$ vector, H_t is an $M \times N$ matrix, and f_t is an $N \times 1$ vector.

In (1) the matrix H_t is time-varying so that it can accommodate the case of a rotation gamma camera in SPECT. In a PET system, however, H_t is stationary, i.e. $H_1 = H_2 = \cdots = H_S$. For convenience, let $\mathbf{H} = diag\,[H_1, H_2, \ldots, H_S]$, $\mathbf{g} = \left[g_1^T, g_2^T, \ldots, g_S^T\right]^T$ and $\mathbf{f} = \left[f_1^T, f_2^T, \ldots, f_S^T\right]^T$. Then (1) can be rewritten in a compact form as

$$E[\mathbf{g}] = \mathbf{H}\mathbf{f} \tag{2}$$

Our goal is to reconstruct the image frames $\mathbf{f}$ from the projection data $\mathbf{g}$.

While it might be possible to apply a traditional reconstruction technique to solve (2) in a frame-by-frame fashion, the reconstruction results are expected to be very noisy because of the reduced data counts for each frame. Moreover, in a slow rotation SPECT system the projection data are far from being complete for reconstruction of each frame, i.e. $M \ll N$. To deal with these problems, below we introduce regularization on the dynamic images to compensate for deficient data counts.

3. REGULARIZED DYNAMIC RECONSTRUCTION

3.1. Imaging model using basis functions

In this paper we model the dynamic behavior of each pixel as a linear combination of a set of nonnegative basis functions as follows

$$f_t(j) = \sum_{k=1}^{K} w_k(j) b_{kt}, \quad t = 1, \ldots, S; \;\; j = 1, \ldots, N \tag{3}$$

where $f_t(j)$ is the j^{th} pixel of frame f_t, b_{kt} denotes the value of the k^{th} basis function at time t, and $w_k(j)$ denotes its corresponding weight at pixel j. With the basis functions pre-defined, the time activity function at each pixel is now determined by their corresponding weights. In practice, K is typically much smaller than S. Thus, the model in (3) can provide a much more compact representation (hence less storage) of the dynamic images.

To simplify the notation, let $w_k = [w_k(1), \ldots, w_k(N)]^T$, i.e., a vector consisting of the weights at all image pixels corresponding to the k^{th} basis function. Moreover, let $\mathbf{w} = \left[w_1^T, \ldots, w_K^T\right]^T$, which is the entire collection of unknown weights for all basis functions.

Define

$$\mathbf{B} = \begin{bmatrix} b_{11} & b_{21} & \cdots & b_{K1} \\ b_{12} & b_{22} & \cdots & b_{K2} \\ \vdots & \vdots & \ddots & \vdots \\ b_{1S} & b_{2S} & \cdots & b_{KS} \end{bmatrix} \otimes I$$

where $\otimes$ denotes the Kronecker product, and I is the $N \times N$ identity matrix. Then, from (3) the dynamic images $\mathbf{f}$ can be written as

$$\mathbf{f} = \mathbf{B}\mathbf{w} \tag{4}$$

Upon substitution of (4) into the the imaging model in (2), we get

$$E[\mathbf{g}] = \mathbf{H}\mathbf{B}\mathbf{w} = \mathbf{H}_\mathbf{B}\mathbf{w} \tag{5}$$

where $\mathbf{H}_\mathbf{B} \equiv \mathbf{H}\mathbf{B}$, which is the system matrix expressed in terms of the unknown weights.

In emission tomography, the tracer distribution is nonnegative. Thus, one can further impose a constraint that the elements of $\mathbf{w}$ are nonnegative [15].

3.2. Regularized maximum-likelihood criterion

Instead solving for $\mathbf{f}$, we determine $\mathbf{w}$ from (6) using regularized maximum-likelihood (ML) estimation, i.e. maximum *a posteriori* (MAP), as

$$\hat{\mathbf{w}} = arg\max_{\mathbf{w}}[\log p(\mathbf{g};\mathbf{w}) + \log p(\mathbf{w})], \text{ subject to } \mathbf{w} \geq 0 \tag{6}$$

where $p(\mathbf{g};\mathbf{w})$ is the likelihood function of the data parameterized by $\mathbf{w}$, and $p(\mathbf{w})$ is a prior distribution on $\mathbf{w}$.

From above, it can be seen that the problem of estimating the unknown weights $\mathbf{w}$ becomes essentially the same as that in traditional image reconstruction, and thus, can be solved by using a traditional MAP reconstruction algorithm. Once $\mathbf{w}$ is determined, $\mathbf{f}$ can then be obtained through the interpolation in (4).

In this study, we used the modified block sequential regularized expectation-maximization (BSREM) algorithm [15] to solve the dynamic reconstruction problem in (6). The details of this reconstruction algorithm can be found in [15].

3.3. Adaptive temporal regularization

We use a Gibbs prior for $\mathbf{w}$

$$p(\mathbf{w}) = \frac{1}{Z}\exp(-\beta U(\mathbf{w})) \tag{7}$$

where Z is a normalization constant, β is a scaling parameter (controlling the strength of the regularization), and $U(\mathbf{w})$ is an energy function enforcing the desired property on the reconstruction.

In this work, we explore a new form of the prior $p(\mathbf{w})$ by exploiting the time-varying statistics of the data. Specifically, we define

$$U(\mathbf{w}) = \sum_{t=1}^{S} \alpha_t \sum_{j=1}^{N} \sum_{i \in \aleph_j} [f_t(j) - f_t(i)]^2 \tag{8}$$

where $\aleph_j$ is the unit-distance neighborhood around pixel j, and α_t is a scaling parameter. The term $U(\mathbf{w})$ is used to enforce local smoothness among neighboring pixels in the same frame. The factor α_t is introduced such that the smoothness

is time-varying (i.e., temporally adaptive) according to the image temporal activities.

Substituting the linear model (3) into the energy function in (8) and upon some algebraic manipulation, we get

$$U(\mathbf{w}) = \sum_{j=1}^{N} \sum_{i \in \aleph_j} \sum_{k=1}^{K} \sum_{k'=1}^{K} c_{kk'}(w_k(j) - w_k(i))(w_{k'}(j) - w_{k'}(i)) \tag{9}$$

where

$$c_{kk'} \equiv \sum_{t=1}^{S} \alpha_t b_{kt} b_{k't} \tag{10}$$

It is interesting to note that the energy function in (9) can be viewed as a more general form of the prior in our previous work [9], where the following spatial energy function was used:

$$U(\mathbf{w}) = \sum_{k=1}^{K} \sum_{j=1}^{N} \sum_{i \in \aleph_j} [w_k(j) - w_k(i)]^2 \tag{11}$$

In (11) all weights of the different basis functions contribute in an equal fashion to the energy function. However, in (9) the weights of the different basis functions are weighted by the cross-correlation between the basis functions. In particular, a weight whose basis function has a larger temporal distribution will have a larger impact on the energy function. Thus, the weights $\mathbf{w}$ will be regularized in an adaptive fashion in the resulting prior.

For convenience, the prior corresponding to (11) will be subsequently referred to as the *Form I* prior, and that corresponding to (9) will be referred to as the *Form II* prior.

4. EVALUATION STUDY

4.1. Methods

To demonstrate the proposed reconstruction approach, we used the gated mathematical cardiac-torso (gMCAT) D1.01 phantom [16] and simulated SPECT acquisition using Tc^{99m} labeled Teboroxime as the imaging agent. Our experiments were based on a single slice of the phantom of the first gate. In addition, a simulated defect was introduced in the myocardium. Both the phantom and the time activity curves (TACs) are shown in Fig. 1. As can be seen, the defect has a slower uptake and washout than the healthy myocardium.

In our simulation, a triple-head camera system was used, and 80 rotation stops covering a total of 480° by each head with 64 projection bins at each stop were used during 12 min data acquisition. The field of view was 40.5 cm. Poisson noise at the count level of total 71,500 counts was introduced. The system had an distance-dependent blur of approximately 13 mm full width at half-maximum (FWHM) at the center. No attenuation and scatter was used.

In this study, we used six cubic B-spline basis functions with the knot placement at $[0, 0, 0, 0, 0.5, 1.5, 12, 12, 12, 12]$ min as in [10]. We chose the temporal weighting parameter α_t in (10) to be inversely-proportional to the time activities

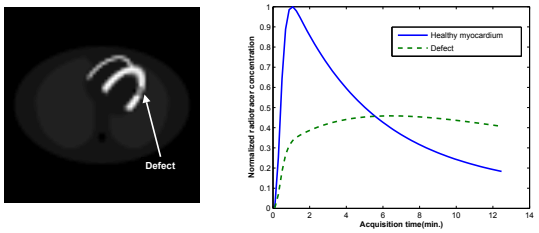

Fig. 1. Simulated Tc99m-Teboroxime dynamic gMCAT phantom.

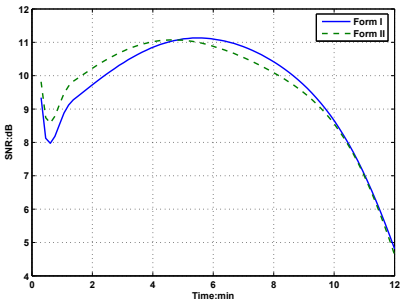

Fig. 2. SNR values for the different regularization methods.

of myocardium, which was averaged inside the heart region from an initial reconstruction using (11).

4.2. Results

The reconstruction algorithm was tested for a wide range of parameters for the different regularization methods. Shown in Fig. 2 is a plot of the obtained signal to noise ratio (SNR) values of the reconstructed dynamic images vs time for the different methods. In this plot, the SNR value was calculated on the myocardium region and averaged over 20 different noise realizations. The parameters used for each method were as follows: 1) $\beta = 3 \times 10^{-6}$ for Form I; 2) $\beta = 2 \times 10^{-7}$ for Form II. These parameters were chosen such that the SNR averaged over time is the best for each method. As can be seen, the Form II prior can lead to higher SNR values in the early stage (where fast dynamic change occurs) than the Form I prior.

In Fig. 3 we show the obtained TACs for the 2×2 regions of interest (ROIs) of the normal myocardium and the defect, respectively, from the reconstructed dynamic images by the different methods. For comparison purposes, the TACs obtained from EM reconstruction using noise-free and complete projection data (denoted as "Ideal") are also shown for the two ROIs. These results show that the Form II method yields more accurate reconstruction of the time activities. It is noted that with Form II prior the TAC of the defect ROI is better separated from that of the normal ROI, which means better differentiation between the defect and normal myocardium.

In Fig. 4, we show some typical reconstructed dynamic images by the different methods for the heart region at time $t = 2$, 5, and 11 min. These images show that the intensity

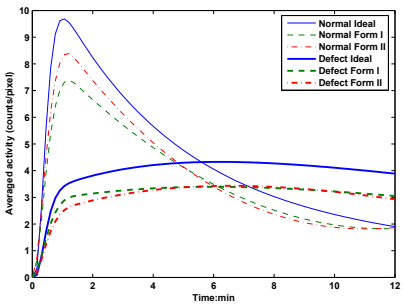

Fig. 3. Reconstructed time activity curves by the different methods.

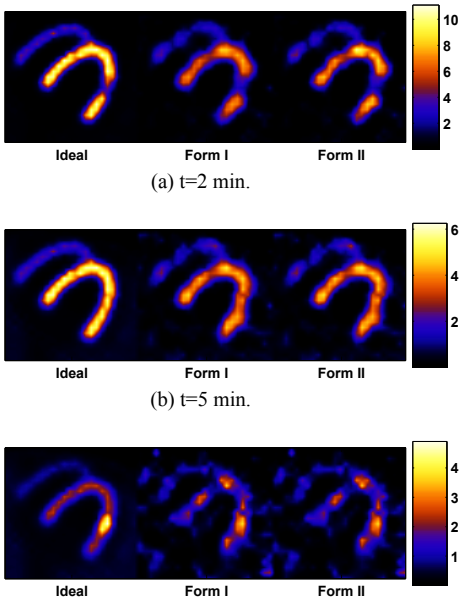

(a) t=2 min.

(b) t=5 min.

(c) t=11 min.

Fig. 4. Reconstructed images by the different methods. Note that the defect is initially dimmer at the early stage (a), but becomes notably brighter than the normal heart wall in the late stage (c).

level of the heart wall is more accurately reconstructed during the early stage with the Form II prior. Note that the introduced defect is initially dimmer at the early stage, but becomes notably brighter than the normal heart wall in the late stage.

5. CONCLUSIONS

In this work we investigated the use of temporal basis functions for dynamic image reconstruction in emission tomography. We proposed an adaptive regularization prior where smoothing is enforced according to the time-varying data statistics. Our experiments show that the proposed approach can yield more accurate reconstruction of the time activities, which is important for differentiation between perfusion defects and the normal myocardium.

6. REFERENCES

[1] D. Snyder, "Parameter estimation for dynamic studies in emission-tomography systems having list-mode data," *IEEE Trans. Nucl. Sci.*, vol. 31, pp. 925–931, 1984.

[2] T. E. Nichols, J. Qi, E. Asma, and R. M. Leahy, "Spatiotemporal reconstruction of list-mode PET data," *IEEE Trans. Med. Imag.*, vol. 21, pp. 396–404, 2002.

[3] B. W. Reutter, G. T. Gullberg, and R. H. Huesman, "Direct least square estimation of spatiotemporal distributions from dynamic SPECT projections using a spatial segmentation and temporal B-splines," *IEEE Trans. Med. Imag.*, vol. 19, pp. 434–450, 2000.

[4] J. Verhaeghe, Y. D'Asseler, S. Vandenberghe, S. Staelens, R. Van de Walle, and I. Lemahieu, "ML reconstruction from dynamic list-mode PET data using temporal splines," in *IEEE Nucl. Sci. Symp. Conference Record*, 2004, pp. 3146–3150.

[5] M. N. Wernick, J. E. Infusino, and M. Milosevic, "Fast spatio-temporal image reconstruction for dynamic PET," *IEEE Trans. Med. Imag.*, vol. 18, pp. 185–195, 1999.

[6] J. Matthews, D. Bailey, P. Price, and V. Cunningham, "The direct calculation of parametric images from dynamic PET data using maximum-likelihood iterative reconstruction," *Phys. Med. Biol.*, vol. 42, pp. 1155–1173, 1997.

[7] T. H. Farncombe, S. Blinder, A. Celler, D. Noll, J. Maeght, and R. Harrop, "A dynamic expectation maximization algorithm for single camera rotation dynamic SPECT (dSPECT)," in *IEEE Nucl. Sci. Symp. Conference Record*, 2000, vol. 2, pp. 15/31–15/35.

[8] M. Jin, Y. Yang, and M. A. King, "Reconstruction of dynamic gated cardiac spect," *Med. Phys.*, vol. 33, pp. 4384–4394, 2006.

[9] E. Gravier and Y. Yang, "Motion-compensated reconstruction of cardiac images," in *IEEE Nucl. Sci. Symp. Conference Record*, 2005, pp. 2364–2367.

[10] E. Gravier, Y. Yang, and M. Jin, "Tomographic reconstruction of dynamic cardiac image sequences," *IEEE Trans. Image Processing*, in press.

[11] Ping-Chun Chiao, W. L. Rogers, N. H. Clinthorne, J. A. Fessler, and A. O. Hero, "Model-based estimation for dynamic cardiac studies using ECT," *IEEE Trans. Med. Imag.*, vol. 13, pp. 217–226, 1994.

[12] E. D. Morris, C. J. Endres, K. C. Schmidt, B. T. Christian, R. F. Muzic Jr, and R. E. Fisher, "Kinetic modeling in positron emission tomography," in *Emission Tomography: The Fundamental of PET and SPECT*, M. N. Wernick and J. N. Aarsvold, Eds., chapter 23, pp. 499–540. Elsevier Academic Press, San Diego, CA, 2004.

[13] M. E. Kamasak, C. A. Bouman, E. D. Morris, and K. Sauer, "Direct reconstruction of kenetic parameter images from dynamic PET data," *IEEE Trans. Med. Imag.*, vol. 24, pp. 636–650, 2005.

[14] R. H. Huesman, B. W. Reutter, G. L. Zeng, and G. T. Gullberg, "Kinetic parameter estimation from SPECT cone-beam projection measurements," *Phys. Med. Biol.*, vol. 43, pp. 973–982, 1998.

[15] S. Ahn and J. A. Fessler, "Globally convergent image reconstruction for emission tomography using relaxed ordered subsets algorithms," *IEEE Trans. Med. Imag.*, vol. 22, pp. 613–626, 2003.

[16] P. H. Pretorius, W. Xia, M. A. King, B. M. W. Tsui, T-S. Pan, and B. J. Villegas, "Evaluation of right and left ventricular volume and ejection fraction using a mathematical cardiac torso phantom for gated blood pool SPECT," *J. of Nucl. Med.*, vol. 38, pp. 1528–1534, 1997.